Article

A Hybrid Molecularly Imprinted Polymer for Selective Adsorption of Urinary S-Phenylmercapturic Acid

Rafaela P. Gomes, [a] *Marina C. Tonucci,*[a] *Maiyara C. Prete,*[b] *César Ricardo T. Tarley,* *,[b,c]
Bruno Eduardo L. Baeta[a] *and Robson J. C. F. Afonso* [a]

*ªDepartamento de Química, Universidade Federal de Ouro Preto (UFOP),
Campus Universitário Morro do Cruzeiro, Bauxita, 35400-000 Ouro Preto-MG, Brazil*

*ᵇDepartamento de Química, Universidade Estadual de Londrina (UEL),
Rodovia Celso Garcia Cid, PR 445, Km 380, 86050-482 Londrina-PR, Brazil*

*ᶜInstituto Nacional de Ciência e Tecnologia em Bioanalítica (INCTBio), Departamento de Química Analítica,
Instituto de Química, Universidade Estadual de Campinas (UNICAMP),
Cidade Universitária Zeferino Vaz Campus s/n, 13083-861 Campinas-SP, Brazil*

A hybrid molecular imprinted polymer (HMIP) obtained by the organic monomer 4-vinylpyridine (4-VP) and the inorganic precursor tetraethyl orthosilicate (TEOS) was synthesized for the selective extraction of urinary S-phenylmercapturic acid (u-SPMA), a biomarker of benzene exposure. The chemical and structural characterization of the synthetic adsorbent was performed by Fourier transform infrared spectroscopy (FTIR), thermogravimetric analysis (TGA), and textural analysis employing N_2 adsorption-desorption isotherms. Selective and adsorptive performance of the imprinted polymers were evaluated by kinetic, isothermal, thermodynamic, and selectivity studies. The kinetic data were well adjusted to pseudo-second order and intraparticle diffusion models, leading to selectivity coefficient (K) value of 0.03 g mg^{-1} min^{-1} for HMIP. In addition, the adsorption isotherms were better described by the Sip model achieving a maximum adsorption capacity of 284.81 µg g^{-1} (at 288.15 K).

Keywords: benzene, S-phenylmercapturic acid, hybrid molecular imprinted polymer, 4-vinylpyridine, tetraethyl orthosilicate

Introduction

In 1987, the International Agency for Research on Cancer (IARC) stated that benzene exposure has sufficient carcinogenic evidence in humans and animals.[1] Since then, limits of exposure to this substance, especially by people who work with it, have been recommended. The urinary S-phenylmercapturic acid (u-SPMA), a benzene metabolite, is a biomarker for benzene exposure, and its concentration can be related to the counts of segmented neutrophils in the blood, an indicator of infection. It was observed that workers with reasonable concentrations of u-SPMA were 4.5 times more likely to have abnormal counts of segmented neutrophils.[2]

Another concern is about non-occupational exposures, in which the main sources are cigarette smoke and gases released by vehicles after gasoline combustion. Thus, exposure to secondhand smoke, living near busy roads, and the use of household heating fuels were also associated with higher levels of benzene metabolites, including the u-SPMA.[3]

Although exposure to benzene has no safety limit, technological advances and new legislation[2,3] have helped to reduce their exposure levels. Also, only 0.11% of the absorbed benzene is biotransformed into u-SPMA. The most used analytical methods for SPMA determination in urine sample extracts are based on high-performance liquid chromatography coupled with mass spectrometry technique (HPLC-MS).[3-6] Although HPLC-MS is a very selective and sensible technique, urine samples are constituted of a diverse biological matrix and the concentration of u-SPMA found in urine samples is very low. Thus, methods of sample preparation are needed before HPLC-MS analysis to reduce the interferences and promote a better sensitivity to the u-SPMA determination.

Solid phase extraction (SPE) is the most common pre-treatment method aimed at quantifying u-SPMA by chromatographic techniques, characterized by ease of operation and effective purification.[7,8] Carbonaceous materials, biosorbents, and modified clay have been used in SPE for the extraction of organic compounds.[9,10] However, in general, some of these materials may have low adsorption capacity, be unstable, and be non-reusable. For the material application as SPE sorbent be feasible, it must have a high adsorption capacity, high surface area, be reusable, chemically resistant, and present robustness in sorption in a wide pH range.

Molecular imprinting technology (MIT) has emerged as a promising alternative capable of developing adsorbent materials that act in the selective removal of a component or impurity in solution. For this, a surface phenomenon occurs at the interface between two phases, which occurs due to the establishment of specific physical or chemical interactions between the adsorbate and the adsorbent.[11] MIT can produce polymers endowed with selective recognition sites and stereochemically molded from the molecule of interest, called a template. This strategy has grown widely and has shown promising results for the development of pre-concentration and/or clean-up methods for analytes in sample extracts.[8,11,12]

Hybrid organic-inorganic polymers combine the advantages of inorganic and organic compounds. Inorganic compounds usually have high chemical and thermal stability, which allows their application under different operating conditions.[13,14] On the other hand, organic compounds are characterized by their versatility and synthetic reactivity, which makes it possible to modulate the molecular structure of a template molecule to increase selectivity concerning a specific target analyte.[15] In this sense, organic-inorganic hybrid polymers have been widely studied as sorbents for SPE aiming at the development of extraction/preconcentration methods of organic species.[11,16-18]

Research has proven that mechanical resistance and chemical stability can be increased by adding inorganic particles to organic materials to form hybrids.[8,12,19,20] Following this idea, the most general synthesis approach has been the exploration of the inorganic compound as a protective matrix in which the organic part is dispersed by different techniques.[15] Thus, organic/inorganic hybrid materials associate the advantages of organic and inorganic counterparts through synergistic or complementary behaviors.[15]

Among the techniques of organic-inorganic hybrids preparation, the sol-gel approach is the most used, where the sol consists of a suspension of colloidal particles (dimension between 1 and 1000 nm) in a liquid and the gel is formed by a rigid structure, and colloidal particles of polymer chains that immobilize the liquid phase in its interstices.[19,21] This synthesis approach involves the hydrolysis and polycondensation of precursors derived from alkoxides.[22]

The inorganic part can be obtained by using various substances, and the synthesis route will be dependent on the nature of this substance. The use of tetraethyl orthosilicate (TEOS) provides the inorganic polymer small particle sizes, high pore volume, and large surface area.[23] In addition, the hydrolysis and condensation of silicon alkoxides is a cost-effective and suitable method to produce silicates, which can be finely dispersed in different polymeric matrices.

The processability at mild temperature, the possibility of adjusting the experimental structure, and the ease of deposition in varied substrates allow precise control of the resulting polymeric material. In addition, the flexibility of sol-gel in the development of hybrid materials promotes the development of a porous structure with a high specific surface area and local concentration of reactive functional groups that results in better analytical sensitivity and selectivity due to rapid mass transport, easy access of the analyte to the connection sites and faster recognition.[22] Thus, this work evaluated the synthesis of a molecular imprinted polymer (HMIP) used as a solid phase of a cartridge extraction for the recovery of SPMA present in urine.

Experimental

Synthesis reagents

All reagents used were of analytical grade without any previous purification. The u-SPMA standard molecule was synthesized according to the methodology described by Zbarsky and Young.[24] For the synthesis of the polymers, the following reagents were used: 4-vinylpyridine (4-VP) (95%) as the organic monomer, trimethylolpropane trimethacrylate (TRIM) as cross-linking agent, tetraethyl orthosilicate (98%) as inorganic reticulant agent, 2,2'-azobis(2-methylpropionitrile) (AIBN) (98%) as radical initiator, and 3-methacryloxypropyltrimethoxysilane > 98% (KH 570) as a coupling agent between the organic and inorganic phases, all obtained by Sigma-Aldrich (Steinheim, Germany). Acetonitrile and ethyl alcohol 99% were obtained from J. T. Baker (Pennsylvania, USA), and hydrochloric acid and dimethylsulfoxide (DMSO) were obtained from Merck (Darmstadt, Germany).

Quantitative analysis of u-SPMA

The chromatographic conditions for u-SPMA determination were employed according to Gomes *et al.*[25]

using HPLC-MS/MS triple quadrupole model Nexera X2 from Shimadzu (Kyoto, Japan), equipped with an automatic sampler (model SIL 30AC), a torque pump system (model LC-30AD) and a column oven (model CTO-30A). The analysis by mass spectrometry was performed by electrospray ionization, operating in negative mode (ESI–), with the temperature of the desolvatation line at 250 °C, the flow of nebulizer gas (N_2) at 3 L min^{-1}, the temperature of the heating block at 400 °C, and the flow of drying gas (N_2) at 15 L min^{-1}, applying −4.5 kV of voltage interface, 16.0 V of the Q1 PRE BIAS, 11.0 V collision energy and 21.0 V of Q1 PRE BIAS. Multiple reaction monitors were used for quantitative analysis of the analyte, in the transition of 238.15 *m/z* (precursor ion) and 109.0 *m/z* (fragment ion).

Molecularly imprinted hybrid polymer (HMIP) synthesis procedure

The synthesis was carried out according to Prete *et al.*[26] with minor modifications. For this, 1.0 mmol of u-SPMA acid (template) was solubilized in 4.0 mL of a mixture of solvents (3.7 mL acetonitrile and 0.3 mL DMSO) in a round bottom glass flask and then, 4.0 mmol of 4-VP was added to the solution. The mixture was kept under magnetic stirring for 30 min at room temperature. Then, 1.5 mmol of TRIM, 2.0 mmol of KH 570, 150 mg of AIBN, 1.0 mmol of TEOS previously diluted in 1.0 mL of ethanol, and 0.38 mL of HCl 1.0 mol L^{-1} were added to the mixture. The solution was bubbled with nitrogen gas for 5 min and the flask was maintained for 24 h under magnetic stirring in a glycerin bath at 60 °C. Subsequently, the resulting product was washed with methanol, 10% acetic acid, and deionized water, and dried at 60 °C for 24 h. Following, the dried material was macerated and sieved to obtain particles size between 32 and 53 μm.

The procedures described above were also performed without the presence of the template molecule to obtain the non-imprinted hybrid polymer (HNIP) used as control.

Chemical and structural characterization of materials

Identification of functional groups in the hybrid polymers was performed by Fourier transform infrared spectroscopy (FTIR), using the conventional potassium bromide (KBr) method, conducted in an ABB Bomem MB 3000 Spectrometer (Quebec, Canada) with a resolution of 4 cm^{-1} and measured between 400 to 4000 cm^{-1} and 32 scans.

Thermogravimetric analysis and their derivatives (TGA/DTG) were performed on SDT2960 equipment PerkinElmer (Massachusetts, USA). For this, about 6.0 ± 0.1 mg of the sample was packed in a hermetically sealed aluminum crucible and analyzed in the range of 20 to 1000 °C, at a heating ratio of 20 °C min^{-1} and in a dynamic atmosphere with constant nitrogen flow.

The morphological characteristics were evaluated by scanning electron microscopy (SEM), using a FEG Scanning Electron Microscope - Quanta 200 FEI/Thermo Fischer Scientific (Eindhoven, Netherlands) equipped with energy dispersive X-ray spectroscopy system (EDS). For SEM analysis, the polymers were fixed with carbon tape and metalized with gold using a metalizing equipment Bal-Tec (Pfäffikon, Switzerland), model MD20, to minimize the load under the incident electron beam. The SEM images of the polymers were obtained in 1000-, 15000-, 35000- and 100000-times magnification with an interval between 9.7 and 10 nm. EDS was used to provide semiquantitative information on the elemental composition of silica (Si) and oxygen (O) atoms present in polymers.

Information on the specific surface area, average pore volume, and size were obtained by N_2 adsorption/desorption isotherms. The measurements were performed on the NOVA-2200 equipment, version 6.11, from Quantachrome (Odelzhausen, Germany), and before measurement, 300 mg of each material was dried under vacuum for 5 h at 50 °C. Specific surface and porosity parameters were obtained for progressive values of relative pressure in the range of 0.05 to 0.99. Once the established relative pressure was reached, the volume of nitrogen adsorbed to form a complete monolayer on the solid surface was determined.

Material performance study

Most SPMA is excreted in the urine in the form of pre-SPMA (*N*-acetyl-*S* (1,2-di-hydro-2-hydroxyphenyl)-L-cysteine). Therefore, it is necessary to adjust the urine samples pH to between 0.5-1.0 by adding 6 mol L^{-1} HCl for the acid hydrolysis of pre-SPMA in u-SPMA with maximum yield.[27] Thus, all aqueous u-SPMA solutions used in material performance studies had pH adjusted to 1.0.

Adsorption performance of HMIP

To evaluate the adsorption performance of the HMIP towards the u-SPME molecule, 24-hour adsorption tests were performed to achieve the adsorption equilibrium. For this task, 5.0 mg of HMIP was added to 1.25 mL of an aqueous solution containing 500 μg L^{-1} of u-SPMA. Then, the mixture was shaken at 150 rpm for 24 h at 25 °C. After that, an aliquot of 150 μL was collected, filtered through a polytetrafluoroethylene (PTFE) 0.20 μm membrane, and analyzed by HPLC-MS/MS according to the methodology

validated by Gomes *et al.*[25] For comparison purposes, the same procedure was carried out with the HNIP.

Based on these experiments, the adsorption performance of the materials was evaluated by calculating the adsorbed amount *per* unit mass of adsorbent (Q_e), the binding percentage (B), the coefficient of distribution (K_d), and the imprinting factor (IF).

Selectivity study

To assess the selectivity of HMIP towards the u-SPMA molecule, 5.0 mg of HMIP or HNIP were stirred for 24 h with 1.25 mL of a binary solution containing u-SPMA and another similar molecule, both at 5 mg L^{-1}. The selected competitive analytes were thioanisol, *S*-phenyl-L-cysteine, *N*-acetylcysteine, and acetaminophen, which have smaller molecular masses and structures very similar to the u-SPMA molecule.

The selectivity was evaluated employing the relative selectivity coefficient (K'), which is calculated according to equations 1 and 2. For K' values greater than 1, it can be inferred that the formation of selective sites for the analyte occurred.

$$K = \frac{K_{d(template)}}{K_{d(competition)}} \tag{1}$$

$$K' = \frac{K_{imprinted\ polymer}}{K_{non\ imprinted\ polymer}} \tag{2}$$

u-SPMA adsorption kinetics

To evaluate the effect of time on u-SPMA adsorption in the hybrid polymer, 1.25 mL of a u-SPMA solution at 500 μg L^{-1} concentration was added to a 10 mL amber vial containing 5.0 mg of HMIP. The vial was placed in a universal shaker (Equipment Thoth model 6430B) and stirred at 150 rpm in times varying from 0.5 to 60 min. After each time, aliquots of 150 μL were collected and filtered through a 0.25 μm PFTE membrane. The amount of u-SPMA adsorbed at each time (Q_e / mg g^{-1}) was calculated and plotted as function of time. The data obtained were fitted to non-linear models of pseudo-first order and pseudo-second order, and linear models of Elovich and intraparticle diffusion.

Adsorption isotherms

To obtain information about the maximum adsorption capacity of the HMIP, 5.0 mg of the hybrid polymer was stirred at 150 rpm with 1.25 mL of u-SPMA solutions at concentrations ranging from 50 to 3000 μg L^{-1} for 3 min. After that, 150 μL of the solution were collected, filtered in a PTFE 0.20 μm membrane, and analyzed by HPLC-MS/MS. This experiment was carried out at temperatures of 288.15; 298.15; 308.15 and 318.15 K. The amount of u-SPMA adsorbed (Q_e / mg g^{-1}) was plotted in function of the supernatant equilibrium concentration (mg L^{-1}). The data obtained were fitted to the non-linear models of Langmuir and Freundlich, as well as to the Sips and Temkin models. The equations corresponding to these models are described by Tonucci and Gurgel.[28]

Effect of temperature on u-SPMA adsorption onto HMIP

To obtain information about the thermodynamics of the adsorption process, parameters as standard Gibbs free energy change ($\Delta_{ads}G°$), enthalpy change ($\Delta_{ads}H°$), and entropy change ($\Delta_{ads}S°$) were calculated. For this, K_d was calculated using the data obtained at isotherm studies for the concentration of 1500 μg L^{-1}. The results were plotted in a Van't Hoff graph (ln$_{kd}$ *versus* 1/T) giving a linear relationship. The values of $\Delta_{ads}H°$ and $\Delta_{ads}S°$ of the adsorptive process were calculated from its angular and linear coefficients, respectively, while $\Delta G°$ was calculated at a specific temperature.

The Originlab[29] program was used for data analysis.

Results and Discussion

Chemical and structural characterization of materials

The obtention of the hybrid polymers and the presence of functional groups were evaluated by FTIR, and the HMIP and HNIP spectra are presented in Figure 1. No difference was observed between the spectra, which suggests that the presence of the template did not change the structure of the polymer.

The broadband at 3375 cm^{-1} is attributed to the stretch of water physically adsorbed. The low-intensity band at 2940 cm^{-1} refers to the symmetrical and asymmetric stretch of carbon sp^3 C−H bonds of the polymeric chain, presenting its overtone at 1410 cm^{-1}. At 1725 cm^{-1} it can be observed a band attributed to the stretch of C=O regarding the cross-linking agent (TRIM) and the coupling agent (KH-570).[30,31] The stretch of C=N and C=C bonds in the 4-VP ring occurs at 1600 cm^{-1}. The stretch of the Si−O−Si and Si−O−H bonds were observed at 1130 and 1015 cm^{-1}. The bands at 810 and 745 cm^{-1} refer to the axial deformation of the C−H bonds of the R$_2$C=CHR chains and the rocking angular deformation of ethyl groups.
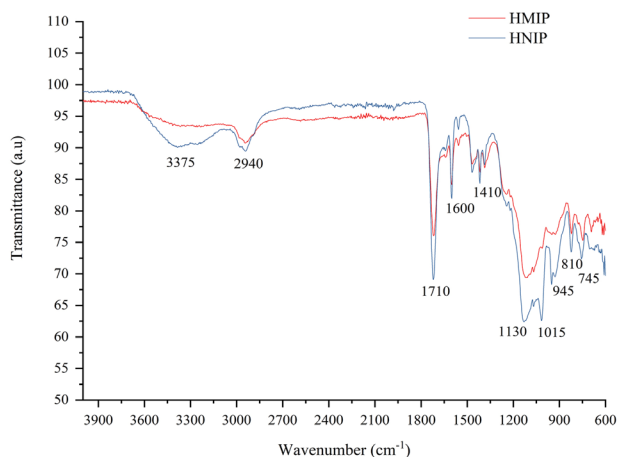
Figure 1. FTIR (KBr) spectra of HMIP and HNIP.

Thermogravimetric analysis of HMIP and HNIP

The thermogravimetric analysis curves are shown in Figure 2, and similar behavior is observed for both HMIP and HNIP. First, there is a degradation of less than 4% up to 100 °C attributed to the desorption of physically adsorbed water.[30] This loss remained almost unchanged up to 300 °C, as can be seen from the first plateau on the graph. The second mass loss event (ca. 40%) took place between 300 and 400 °C and can be assigned to the decomposition of 4-VP chains. The third event is observed between 400 and 500 °C with about 55% of mass loss and is related to the decomposition of the cross-linking agent (TRIM).[30]
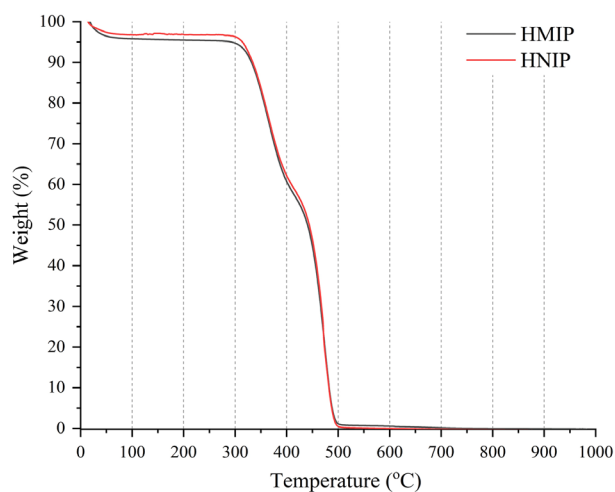
Figure 2. Thermogravimetric behavior of HMIP and HNIP.

Textural parameters of HMIP and HNIP

Textural parameters such as surface area (m² g⁻¹), average pore volume (cm³ g⁻¹), and diameter (nm) are shown in Table 1. It was observed that the HNIP presented a surface area 100× higher than the HMIP, and a pore volume about 148 times higher. This morphological difference may be related to the presence of the template in the polymerization, which may lead to an increase in the solubility of the template-monomer complex in the solvent. As a result, the removal of the porogenic solvent from the polymer interstices is harder, and consequently, there is a lower volume of pores and surface area.[32] Since the materials presented pore sizes between 2 and 50 nm, they can be classified according to International Union of Pure and Applied Chemistry (IUPAC) as mesoporous materials.[33]

Table 1. Textural parameters of surface area, pore volume, and diameter for HMIP and HNIP adsorbents obtained by N_2 sorption/desorption isotherms

Polymer	Surface area / (m² g⁻¹)	Pore volume × 10⁻³ / (cm³ g⁻¹)	Pore diameter / nm
HNIP	96.12	319.70	6.65
HMIP	0.92	2.16	4.67

HNIP: non-imprinted hybrid polymer; HMIP: hybrid molecular imprinted polymer.

Scanning electron microscopy (SEM)

The morphology of the hybrid polymers was evaluated by scanning electron microscopy at magnifications of 1000, 15000, 35000, and 100000 times (Figure 3). The polymers HNIP and HMIP were morphologically similar, being formed by agglomerates of particles. However, it can be observed that the HNIP presents a rougher surface than the HMIP, corroborating with the N_2 sorption/desorption data.

Comparison of HMIP and HNIP adsorptive performance

To evaluate the recognition capacity of HMIPs the binding percentage (B), the distribution coefficient (K_d) and the imprinting factor (IF) were calculated. The binding capacity of the HMIPs was determined by the distribution coefficient and the imprinting factor (IF), which represents the degree of imprinting achieved when comparing the K_d values of the HMIPs with the K_d of the HNIPs. Table 2 presents these parameters.

The HMIP presented an IF of 1.89 indicating that it adsorbs the target molecule with selectivity.[32] The evaluated materials had a high percentage of linkage with the template, 95.04% for HMIP and 90.45% for HNIP.

Q_e values were determined in triplicate and their variance shown in Table 2. Applying the bilateral *t*-test for two samples and assuming equivalent variances, with 95% confidence, we can state that the Q_e means of HMIP and HNIP are different. That is, *p*-value (0.000932) is less than 0.05, therefore H_1 is accepted.

(a)

(b)
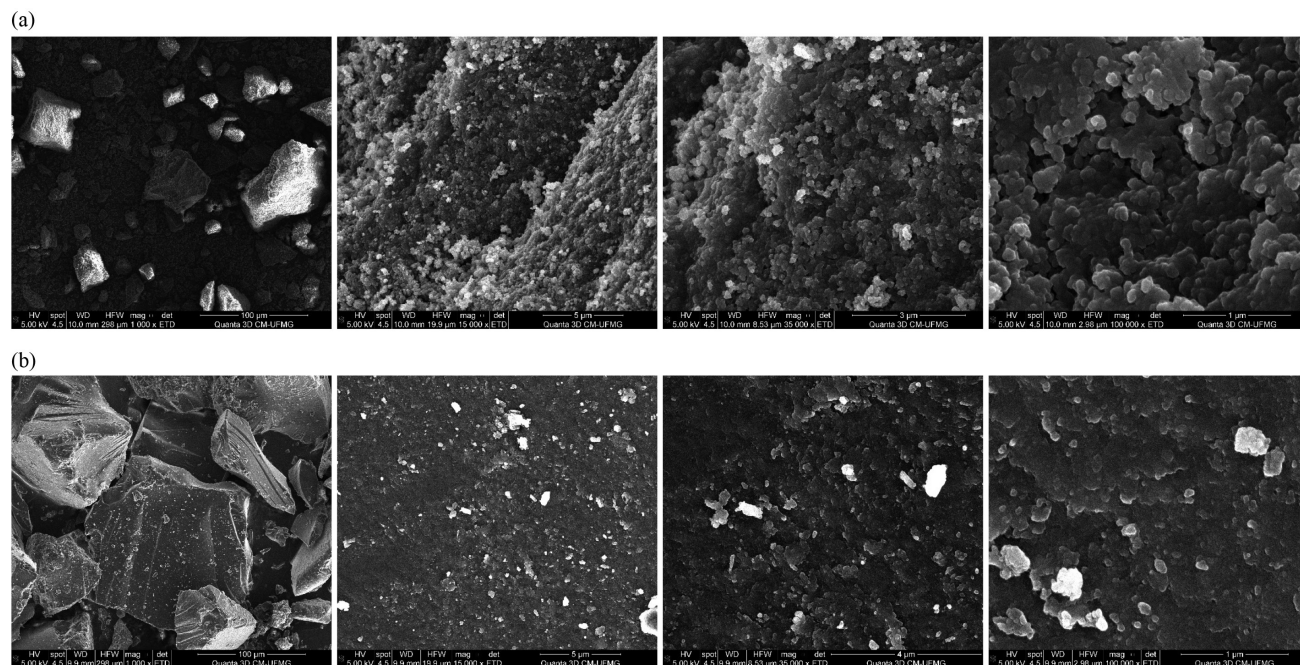
Figure 3. Scanning electron microscopy images at magnifications of 1000×, 15000×, 35000×, and 100000×, respectively, of HNIP (a) and HMIP (b) polymers.

Table 2. Comparison of adsorptive performances of hybrid materials on silica surface

Sample	Q_e variance / ($\mu g\ g^{-1}$)	B / %	K_d / (g L^{-1})	IF
HNIP	104.12 ± 0.18	90.45	2.36	1.89
HMIP	114.26 ± 3.83	95.04	4.47	

HNIP: non-imprinted hybrid polymer; HMIP: hybrid molecular imprinted polymer; Q_e: adsorbed amount *per* unit mass of adsorbent; B: binding percentage; K_d: coefficient of distribution; IF: imprinting factor.

Table 3. Comparison of adsorptive performances of hybrid materials on silica surface considering adsorptive capacity in specific equilibrium

Sample	Q_e variance / ($\mu g\ m^{-2}$)	B / %	K_d / (L m^{-2})	IF
HNIP	1.08 ± 0.18	90.45	0.02	197.76
HMIP	124.17 ± 3.83	95.04	4.86	

HNIP: non-imprinted hybrid polymer; HMIP: hybrid molecular imprinted polymer; Q_e: adsorbed amount *per* unit mass of adsorbent; B: binding percentage; K_d: coefficient of distribution; IF: imprinting factor.

However, the amount of u-SPMA the Q_e of HNIP and HMIP were very close, which could suggest that these adsorptions do not occur due to the formation of selective sites for the target molecule. However, although HMIP has a smaller surface area and a smaller pore volume, it has higher sorption capacity of S-phenylmercapturic acid compared to HNIP. Considering the difference between the surface areas of the materials, it is pertinent to evaluate the amounts of u-SPMA adsorption in the equilibrium performing normalization in relation to the surface area of the material. For this, The Q_e and K_d were calculated using the surface area contained in the mass used for HMIP and HNIP, according to equations 3 and 4. The results obtained are shown in Table 3.

$$Q_e = (C_i - C_e) \times \frac{V(L)}{m(g)} \times \frac{1}{\text{Surface area} \ (m^2 g^{-1})} \quad (3)$$

$$K_d = \left[\frac{(C_i - C_e)}{C_e}\right] \times \frac{V(L)}{m(g)} \times \frac{1}{\text{Surface area} \ (m^2 g^{-1})} \quad (4)$$

where K_d, C_i, C_e, V, and m represent the distribution coefficient, initial concentration, equilibrium concentration, solution volume, and mass of polymers used during the adsorption equilibrium assay, respectively.

When the adsorptive capacity is correlate with the surface area, we have an adsorptive capacity *per* m^2 about 115 times greater for the HMIP, even though its surface area is significantly smaller than the HNIP. The binding percentage (B) does not change, since this variable is dependent only on the initial and equilibrium concentrations of the evaluated analyte.

The parameter related to the affinity between template and adsorbent (K_d) was about 197 times higher for HMIP concerning HNIP. Also, the IF calculated was 197.76, which can be considered high.[34] Therefore, these data suggest that the higher adsorption on HMIP regarding the HNIP occurred as a function of the formation of selective binding sites for the target molecule.

Selectivity study

To evaluate the selectivity of HMIP towards the u-SPMA molecule, competitive adsorption assays were carried out by using binary solutions of u-SPMA:concomitant (1:1 m/m), for both HMIP and HNIP. Molecules with similar structures such as acetaminophen, *S*-phenyl-L-cysteine, *N*-acetylcysteine, and thioanisol were evaluated. In the Supplementary Information (SI) section, the chemical structures of the concomitants were illustrated in Table S1.

The amount of u-SPMA and competing analyte adsorbed at equilibrium (Q_e mg g^{-1}) for both HMIP and HNIP is shown in Figure 4. It is possible to observe that both materials can adsorb the concomitant molecules. However, although HMIP and HNIP presented similar Q_e regarding the u-SPMA adsorption (1078.16 and 1029.38 µg g^{-1}, respectively), a large difference is observed for all competing analyses. For example, HNIP can adsorb
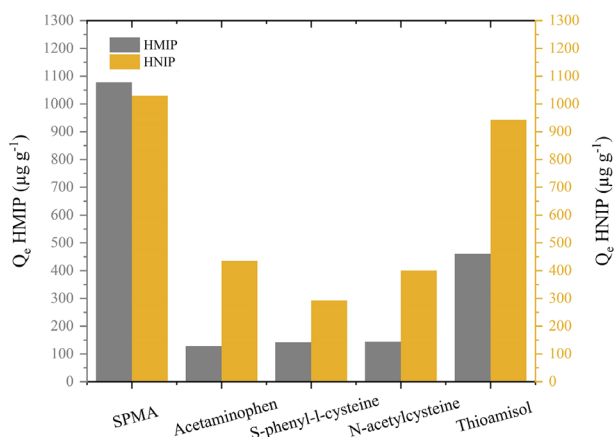
up to 339.2% more acetaminophen when compared with HMIP. Thus, it can be inferred that the high surface area of HNIP allows the adsorption of other molecules, while the binding sites of HMIP promote selective adsorption of u-SPMA regarding the concomitants.

The coefficients of distribution (K_d), selectivity coefficient (K), and relative selectivity coefficient (K') are presented in Table 4. Analyzing K for the binary solution u-SPMA:thioanisol, it is noted that HMIP adsorbs less thioanisol when compared to HNIP, suggesting a pronounced selectivity in the region of the aromatic ring of the analyte. The same adsorptive behavior is observed for acetaminophen, *S*-phenyl-L-cysteine, and *N*-acetylcysteine. These results, together with the K' higher than 1, prove the formation of selective sites for the analyte. Therefore, it can be inferred that the sorption of u-SPMA in HMIP is selective and is not affected by the presence of similar molecules.

Thus, kinetic, isothermal, and thermodynamic were performed only for HMIP.

u-SPMA adsorption kinetics

The u-SPMA adsorption kinetic profile on the HMIP is shown in Figure 5. It was observed that the time required to reach the adsorption equilibrium was 3 min. The value of experimental adsorption capacity (Q_e) was found to be 114.15 µg g^{-1}. The equilibrium time obtained by HMIP is very satisfactory for the application of this material in an SPE cartridge, since its maximum adsorption occurs in a short time, which allows higher analytical frequencies.

To elucidate the mechanisms of the adsorptive process, non-linear pseudo-first, and pseudo-second-order models, and linear models of Elovich and Intraparticle diffusion were applied to the experimental data, and their respective

Figure 4. Amount of u-SPMA and competing molecules (µg g^{-1}) adsorbed at both HMIP and HNIP using binary solutions (5 mg L^{-1}).

Table 4. Selectivity parameters for competitive adsorption on HMIP and HNIP

	u-SPMA	Acetaminophen	S-phenyl-L-cysteine	*N*-Acetylcysteine	Thioanisol
			K_d / (L g^{-1})		
HMIP	4.0809	0.0280	0.0294	0.0310	0.1602
HNIP	3.3025	0.1368	0.0713	0.1159	1.4969
			K		
HMIP	–	145.87	138.80	131.82	25.47
HNIP	–	24.14	46.30	28.51	2.21
			K'		
	–	6.04	3.00	4.62	11.54
			Q_e / (µg g^{-1})		
HMIP	1078.16	128.04	141.55	143.62	460.95
HNIP	1029.38	434.34	293.07	400.55	942.97

u-SPMA: urinary S-phenylmercapturic acid; HMIP: hybrid molecular imprinted polymer; HNIP: non-imprinted hybrid polymer; K_d: coefficient of distribution; K: selectivity coefficient; K': relative selectivity coefficient; Q_e: adsorbed amount *per* unit mass of adsorbent.
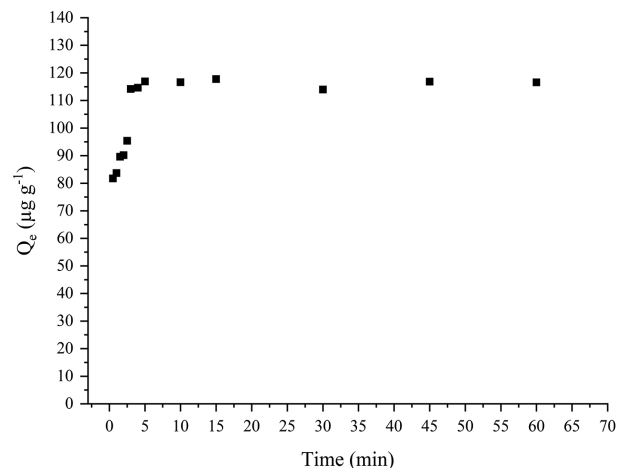
Figure 5. Evaluation of HMIP adsorption capacity (µg g⁻¹) of u-SPMA in function of time (min) using standard solution 500 µg L⁻¹.

reaction, which is related to the gradual sorption inside the material, known as intraparticle diffusion. The third slope indicates the step at which the sorption equilibrium is reached. The intercept of the first line is represented by the intraparticle diffusion constant (C), which is proportional to the thickness of the boundary layer (µg g⁻¹). When C has positive values and does not pass through the origin, it means that the intraparticle diffusion process is not the only one responsible for the sorption process, as the adsorption also occurs on the surface. From the data presented in Table 5, it can be inferred that the sorption of the u-SPMA also occurs on the external surface of the material, since the value of the constant C was positive (104.55 µg g⁻¹).

Adsorption isotherms

Figure 6 shows the adsorption isotherms at different temperatures obtained for the HMIP. The values of Q_e at temperatures of 288.15, 298.15, 308.15 and 318.15 K were 284.81, 332.12, 421.37, and 521.24 µg g⁻¹, respectively. Thus, since the u-SPMA adsorbed increases with temperature, it is considered a favorable endothermic process. Therefore, it can be assumed that, as the temperature increases, the viscosity of the solution decreases, which increases the diffusion of the solution in the outer and inner limit layers of the adsorbent particles.[35,36]

The obtained experimental data were fitted to the non-linear models of Langmuir and Freundlich, as well as the Sips and Temkin models. The fitting of the models to the experimental data is shown in Figure S3 (SI section). The parameters obtained for the fitted models are shown in Table 6.

parameters are presented in Table 5. In the SI section, the graphs with the fitted models were presented in Figures S1 and S2.

Considering the coefficient of determination (R^2), NRMS (normalized root mean square), and theoretical Q_e, it is possible to observe that the non-linear pseudo-second-order model presented the best fit to the experimental data. This model assumes the existence of sites with different energies, and that the sorption velocity is proportional to the square of the number of unoccupied sites.

In the Q_t *vs.* $t^{1/2}$ graph obtained by applying the intraparticle diffusion model, it was possible to observe three inclinations, indicating that three steps occurred in the mass transport. The first slope refers to the diffusion of the analyte from the solution to the outer surface of the material. The second slope is defined as the determining step of the

Table 5. Calculated parameters for the models applied in the data obtained by the sorption kinetics studies for HMIP, $Q_{e \text{ (experimental)}}$: 114.15 µg g⁻¹

	Pseudo-first order			
	K_1 / min⁻¹	Q_e / (µg g⁻¹)	R^2	NRMS
HMIP	0.27 ± 0.04	38.15 ± 2.40	0.9429	4.03×10^{-1}
	Pseudo-second order			
	K_2 / (g mg⁻¹ min⁻¹)	Q_e / (µg g⁻¹)	R^2	NRMS
HMIP	0.03 ± 0.01	117.09 ± 0.51	0.9998	0.14×10^{-1}
	Elovich			
	α / (µg g⁻¹ min⁻¹)	β / (g µg⁻¹)	R^2	NRMS
HMIP	873078.06 ± 2.29 × 10⁶	0.13 ± 0.03	0.6698	7.71×10^{-1}
	Intraparticle diffusion			
	K_{id} / (µg g⁻¹ min⁻¹ᐟ²)	C / (µg g⁻¹)	R^2	NRMS
HMIP	15.39 ± 2.33	69.87 ± 2.85	0.9357	2.10
	5.37 ± 2.27	104.55 ± 4.53	0.8485	1.79

HMIP: hybrid molecular imprinted polymer; Q_e: amount of u-SPMA sorbed at equilibrium time; K_1: pseudo-first order constant; K_2: pseudo-second order constant; α: initialsorption velocity rate; β: is related to surface coverage extension; K_{id}: internal diffusion coefficient; C: constant related to the thickness of the limit layer; R^2: coefficient of determination; NRMS: normalized root mean square.
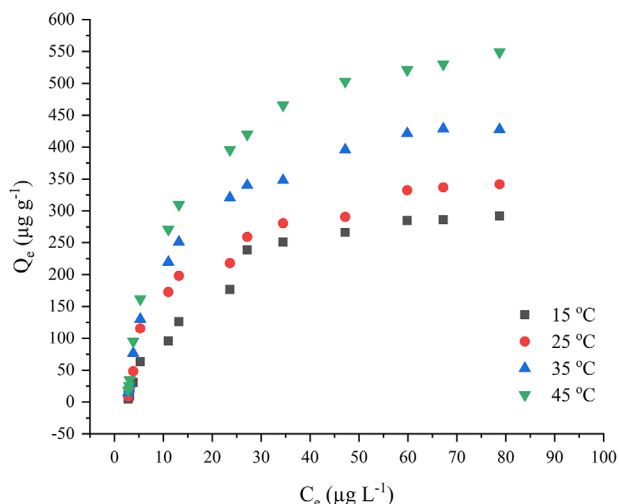
Figure 6. u-SPMA adsorption isotherms on HMIP was carried out at temperatures of 288.15, 298.15, 308.15 and 318.15 K and initial concentration of SPMA ranging from 50 to 3000 µg L^{-1}.

The best fit to experimental data was obtained by the Sips model. This model comprises Langmuir and Freundlich parameters and admits that interactions can occur with different affinities, that is, it considers that the adsorbent has a heterogeneous surface and different interactions towards the u-SPMA molecule. This can be confirmed by evaluating the values of n. When n is equal to 1, the system is considered homogeneous and follows the Langmuir model. However, if the value of n is different

from 1, it means that the system has heterogeneous sites, which can be more energetic and specific, as well as less energetic and non-specific sites. From the data obtained for Sip fitting, n is higher than 1, thus indicating the formation of more than one adsorption site.[37,38]

In addition, the Sips model better describes isotherms in which low concentrations of analyte are adsorbed (initial linear inclination of isotherm) or when saturation of adsorbent concentrations occurs. In the latter case, adsorption occurs in a monolayer with adsorbent saturation, characteristic of Langmuir isotherm.[35,38]

Effect of temperature on u-SPMA adsorption onto HMIP

The thermodynamic parameters obtained by Van't Hoff's equation are shown in Table 7. Van't Hoff's plot is depicted in Figure S4 (SI section).

The Gibbs' free energy ($\Delta_{ads}G°$) values obtained were negative for all temperatures, indicating that the process is spontaneous.[35] With the increase in temperature, more negative values of $\Delta_{ads}G°$ are observed, proving that the adsorption is more energetically favored, as observed in the adsorption isotherms.

The positive values obtained for $\Delta_{ads}H°$ express that the adsorption of u-SPMA is endothermic. In addition, the value of $\Delta_{ads}H°$ provides information about the types of interactions that may occur, such as adsorbate-adsorbate,

Table 6. Calculated parameters for the models applied to the experimental data obtained in the adsorption isotherm studies for u-SPMA adsorption on HMIP

Polymer	Temperature / K	Model	Q_{max} / (µg g^{-1})	K_L / (L µg^{-1})	K_F / (mg g^{-1} L g^{-1})	b / (L µg^{-1})	n	A_T / (L µg^{-1})	R^2	NRMS
HMIP	288.15	LAN	651.45	0.01					0.9474	4.23
		FRE			12.07		1.31		0.9203	4.81
		Sips	302.03			7.90×10^{-4}	2.35		0.9961	4.11
		TEM				119.86		0.17	0.9879	8.85
HMIP	298.15	LAN	765.50	0.01					0.9354	3.75
		FRE			14.71		1.33		0.9094	4.62
		Sips	346.62			1.07×10^{-3}	2.25		0.9767	2.34
		TEM				145.94		0.15	0.9863	9.48
HMIP	308.15	LAN	422.21	0.004					0.9448	6.78
		FRE			45.23		1.86		0.8805	9.02
		Sips	422.21			5.40×10^{-3}	2.05		0.9860	2.89
		TEM				143.12		0.31	0.9777	1.98
HMIP	318.15	LAN	717.81	0.05					0.9710	9.93
		FRE			67.11		1.97		0.9078	12.17
		Sips	564.32			2.04×10^{-2}	1.55		0.9891	7.40
		TEM				162.44		0.45	0.9911	7.18

HMIP: hybrid molecular imprinted polymer; LAN: Langmuir; FRE: Freundlich; TEM: Temkin; Q_{max}: maximum adsorption capacity; K_L: Langmuir equilibrium constant; K_F: Freundlich equilibrium constant; b: Sips empiric constant; n: Freundlich empiric constant; A_T: binding constant at equilibrium; R^2: coefficient of determination; NRMS: normalized root mean square.

Table 7. Thermodynamic parameters of HMIP adsorption processes

Polymer	Parameter	Temperature / K			
		288.15	298.15	308.15	318.15
	$\Delta_{ads}H^o$ / (kJ mol^{-1})	14.16			
HMIP	$T\Delta_{ads}S^o$ / (kJ mol^{-1})	17.78	18.39	19.01	19.63
	$\Delta_{ads}G^o$ / (kJ mol^{-1})	−3.62	−4.23	−4.85	−5.47

HMIP: hybrid molecular imprinted polymer; $\Delta_{ads}H^o$: enthalpy change; $T\Delta_{ads}S^o$: product of temperature and entropy change; $\Delta_{ads}G^o$: standard Gibbs free energy change.

adsorbent-adsorbate, water-adsorbate, and water-adsorbent. Therefore, considering that the $\Delta_{ads}H^\circ$ value is less than 40 kJ mol^{-1} (14.16 kJ mol^{-1}), the adsorption mechanism can be described as physisorption. In this case, the analyte binding on the HMIP surface involves relatively weak interactions that can be attributed to van der Waals forces, which are similar to molecular cohesion forces.[35] Thus, the intermolecular attraction forces of the molecules in the liquid phase and the molecules adsorbed on the adsorbent are greater than the attractive forces between the molecules of the fluid itself.[39] This type of adsorption is fast, reversible, and occurs across the adsorbent surface, so it is considered unlocalized. In addition, the physisorption process allows the formation of several layers of adsorbed molecules. This data corroborates with the values of n greater than 1 in the Sips isotherm, indicative of the formation of more than one layer of analyte on the adsorbent.[37,38]

The obtained positive entropy ($\Delta_{ads}S^\circ$) indicates an increase in the degree of freedom in the system, due to the deconfiguration of u-SPMA molecules by the water molecules, followed by its adsorption on the HMIP. For a process to be spontaneous, the following condition must be met:

$$\Delta_{ads}G^\circ = \Delta_{ads}H^\circ - T\Delta_{ads}S^\circ < 0 \qquad (5)$$

In the present study, $T\Delta_{ads}S^\circ > \Delta_{ads}H^\circ$, so it can be stated that the increase in the degree of freedom in the adsorbent interphase guides the adsorption process, that is, it is an entropically directed process.

Conclusions

This work demonstrates for the first time the synthesis of a hybrid polymer with molecular imprinting for the selective recognition of urinary u-SPMA. The characterization of the HMIP and HNIP by FTIR, TGA, and SEM was useful to confirm the polymerization of organic and inorganic fractions, to inform about the thermal stability of the sample indicating that the materials are thermostable up to 300 °C and present morphological differences between HNIP and HMIP, respectively. The insertion of the coupling agent KH-570 and TEOS as an inorganic crosslinking agent proved to be effective in generating particles with controlled and stable physical properties, with lower sphericity and capable of being used as a stationary phase in cartridges used for extraction in solid phase. Kinetic studies showed that the time required for the u-SPMA achieves equilibrium between the solid phase and the liquid phase was 3 min and the value of experimental adsorption capacity (Q_e) observed of 114.15 µg g^{-1} for HMIP, a fact that favors its application in cartridges for SPE. Finally, with the results obtained, it was possible to synthesize a selective material that has interesting characteristics to be applied as an adsorbent material in the extraction of urinary u-SPMA.

Supplementary Information

Supplementary information (molecular structures, adjustments of kinetic models and adsorption isotherms) is available free of charge at http://jbcs.sbq.org.br as PDF file.

Acknowledgments

Author Contributions

Rafaela P. Gomes was responsible conceptualization, data curation, investigation, validation, visualization, writing original draft, writing-review and editing; Marina C. Tonucci for conceptualization and data curation; Maiyara C. Prete for visualization and writing-review; César Ricardo T. Tarley, Bruno Eduardo L. Baeta and Robson J. C. F. Afonso for conceptualization, data curation, investigation, writing-review and editing.

References

1. World Health Organization International, Agency for Research on Cancer; *IARC Monographs on the Evaluation of Carcinogenic Risks to Humans*; WHO: Lyon, 1987. [Link] accessed in March 2023

2. Agustina, L.; Wulandari, R. A.; *Public Health Indonesia* **2019**, *5*, 138. [Crossref]

3. Schwedler, G.; Murawski, A.; Schmied-Tobies, M. I. H.; Rucic, E.; Scherer, M.; Pluym, N.; Scherer, G.; Bethke, R.; Kolossa-Gehring, M.; *Environ. Res.* **2021**, *192*, 110295. [Crossref]

4. Lovreglio, P.; de Palma, G.; Barbieri, A.; Andreoli, R.; Drago, I.; Greco, L.; Gallo, E.; Diomede, L.; Scaramuzzo, P.; Ricossa, M. C.; Fostinelli, J.; Apostoli, P.; Soleo, L.; *Biomarkers* **2018**, *23*, 70. [Crossref]

5. Frigerio, G.; Campo, L.; Mercadante, R.; Mielżyńska-švach, D.; Pavanello, S.; Fustinoni, S.; *Int. J. Environ. Res. Public Health* **2020**, *17*, 1801. [Crossref]

6. Lovreglio, P.; Stufano, A.; Andreoli, R.; Tomasi, C.; Cagnazzi, P.; Barbieri, A.; Soleo, L.; de Palma, G.; *Toxicol. Lett.* **2020**, *331*, 235. [Crossref]

7. Carrieri, M.; Pigini, D.; Martinelli, A.; Paci, E.; Maratini, F.; Salamon, F.; Tranfo, G.; *Int. J. Environ. Res. Public Health* **2019**, *16*, 129. [Crossref]

8. Luo, L.; Feng, W.; Hu, W.; Chen, C.; Gong, H.; Cai, C.; *Methods Appl. Fluoresc.* **2019**, *7*, 015006. [Crossref]

9. Chu, S.; Haffner, G. D.; Letcher, R. J.; *J. Chromatogr. A* **2005**, *1097*, 25. [Crossref]

10. Ahmadkhaniha, R.; Salimi, M.; Rastkari, N.; *Fullerenes, Nanotubes, Carbon Nanostruct.* **2013**, *21*, 604. [Crossref]

11. Tang, W.; Li, G.; Row, K. H.; Zhu, T.; *Talanta* **2016**, *152*, 1. [Crossref]

12. Beltran, A.; Borrull, F.; Marcé, R. M.; Cormack, P. A. G.; *TrAC, Trends Anal. Chem.* **2010**, *29*, 1363. [Crossref]

13. Zhong, M.; Wang, Y. H.; Wang, L.; Long, R. Q.; Chen, C. L.; *J. Ind. Eng. Chem.* **2018**, *66*, 107. [Crossref]

14. Zhong, M.; Wang, Y.-H.; Wang, L.; Long, R.-Q.; Chen, C.-L.; *J. Sep. Sci.* **2018**, *41*, 3318. [Crossref]

15. Wang, S.; Kang, Y.; Wang, L.; Zhang, H.; Wang, Y.; Wang, Y.; *Sens. Actuators, B* **2013**, *182*, 467. [Crossref]

16. Li, X.; Row, K. H.; *Anal. Sci.* **2017**, *33*, 611. [Crossref]

17. Anacleto, S. D. S.; de Oliveira, H. L.; da Silva, A. T. M.; do Nascimento, T. A.; Borges, M. M. C.; Silva, R. C. D. S.; Pereira, A. C.; Borges, K. B.; *J. Chromatogr. Sci.* **2019**, *57*, 671. [Crossref]

18. Casarin, F.; Dourado, C. S.; Sousa, L. S.; Grassi, M. T.; Dias, A. C. B.; *J. Braz. Chem. Soc.* **2021**, *32*, 1789. [Crossref]

19. José, N. M.; Prado, L. A. S. A.; *Quim. Nova* **2005**, *28*, 281. [Crossref]

20. Song, Y. P.; Li, N.; Zhang, H. C.; Wang, G. N.; Liu, J. X.; Liu, J.; Wang, J. P.; *Food Chem.* **2017**, *233*, 422. [Crossref]

21. Tarley, C. R. T.; Andrade, F. N.; de Oliveira, F. M.; Corazza, M. Z.; de Azevedo, L. F. M.; Segatelli, M. G.; *Anal. Chim. Acta* **2011**, *703*, 145. [Crossref]

22. Ayankojo, A. G.; Reut, J.; Öpik, A.; Furchner, A.; Syritski, V.; *Biosens. Bioelectron.* **2018**, *118*, 102. [Crossref]

23. Malek, S. K.; Nodeh, H. R.; Akbari-Adergani, B.; *J. Sep. Sci.* **2018**, *41*, 2934. [Crossref]

24. Zbarsky, S. H.; Young, L.; *J. Biol. Chem.* **1943**, 211.

25. Gomes, R. D. P.; Pena, C. B.; Rezende, J.; Coutrim, M. X.; Afonso, R. J. D. C. F.; *J. Sep. Sci.* **2017**, *40*, 550. [Crossref]

26. Prete, M. C.; Tarley, C. R. T.; *Chem. Eng. J.* **2019**, *367*, 102. [Crossref]

27. Sterz, K.; Köhler, D.; Schettgen, T.; Scherer, G.; *J. Chromatogr. B* **2010**, *878*, 2502. [Crossref]

28. Tonucci, M. C.; Gurgel, L. V. A.; de Aquino, S. F.; *Ind. Crops Prod.* **2015**, *74*, 111. [Crossref]

29. *Origin(PRO)*, version 2022; OriginLab Corporation, Northampton, MA, USA, 2022.

30. da Fonseca, R. J.; Segatelli, M. G.; Borges, K. B.; Tarley, C. R. T.; *React. Funct. Polym.* **2015**, *93*, 1. [Crossref]

31. Suquila, F. A. C.; de Oliveira, L. L. G.; Tarley, C. R. T.; *Chem. Eng. J.* **2018**, *350*, 714. [Crossref]

32. de Oliveira, F. M.; Segatelli, M. G.; Tarley, C. R. T.; *J. Appl. Polym. Sci.* **2016**, *133*, 1. [Crossref]

33. Sing, K. S. W.; Everett, D. H.; Haul, R. A. W.; Moscou, L.; Pierotti, R. A.; Rouquerol, J.; Siemieniewska, T.; *Pure Appl. Chem.* **1985**, *57*, 603. [Crossref]

34. Liu, L.; Cao, Y.; Ma, P.; Qiu, C.; Xu, W.; Liu, H.; Huang, W.; *RSC Adv.* **2014**, *4*, 605. [Crossref]

35. do Nascimento, R. F.; de Lima, A. C. A.; Vidal, C. B.; Melo, D. Q.; Raulino, G. S. C.; *Adsorção Aspectos Teóricos e Aplicações Ambientais*; Editora UFC: Fortaleza, 2014, p. 78.

36. Tonucci, M. C.; Fidélis, A. L. S.; Baêta, B. E. L.; Tarley, C. R. T.; de Aquino, S. F.; *Polym. Int.* **2019**, *68*, 428. [Crossref]

37. Theodoridis, G.; Kantifes, A.; Manesiotis, P.; Raikos, N.; Tsoukali-Papadopoulou, H.; *J. Chromatogr. A* **2003**, *987*, 103. [Crossref]

38. Saavedra, L. N. M.; Penido, R. G.; Santos, L. A.; Ramalho, T. C.; Baeta, B. E. L.; Pereira, M. C.; da Silva, A. C.; *RSC Adv.* **2018**, *8*, 28775. [Crossref]

39. Sulitzky, C.; Ruckert, B.; Hall, A. J.; Lanza, F.; Unger, K.; Sellergren, B.; *Macromolecules* **2002**, *35*, 79. [Crossref]